

Photoconductivity study of free-carrier, phonon-assisted, and impurity transitions in InSb at magnetic fields up to 20 T

R. Grisar* and H. Wachernig†

Max-Planck-Institut für Festkörperforschung, Hochfeldmagnetlabor, 166 X, 38042 Grenoble Cédex, France

G. Bauer

Experimentelle Physik IV, Universität Ulm, 79 Ulm-Donau, Federal Republic of Germany

J. Wł̄asak

Institute of Physics, Wrocław Technical University, Wrocław, Poland

J. Kowalski and W. Zawadzki

Institute of Physics, Polish Academy of Sciences, Warszawa, Poland

(Received 13 December 1977)

Intraband photoconductivity of high-purity *n*- and *p*-type InSb ($n_{e,h} \approx 10^{13} \text{ cm}^{-3}$) induced by CO₂ laser radiation has been investigated in magnetic fields up to 20 T, exhibiting a number of sharp resonances. These are shown to be associated with free-electron and LO-phonon-assisted spin-conserving and spin-flip transitions as well as impurity excitations. Phonon-assisted hole transitions have been also observed. The selection rules for intraband and interband excitations, calculated for $\vec{H} \parallel [100]$ direction and including k_z terms, warping, and inversion asymmetry, account for most of the observed resonances. A corrected Pidgeon and Brown scheme with the band parameters $\gamma_1^t = 31.1$, $\gamma_2^t = 14.3$, $\gamma_3^t = 15.4$, $\kappa^t = 13.9$, $E_p = 21.6 \text{ eV}$, $\epsilon_g = 0.2355 \text{ eV}$, and $\Delta = 0.803 \text{ eV}$ describes well the free-electron and phonon-assisted transition energies in both bands as well as interband and intraband magneto-optical data of other authors.

I. INTRODUCTION

In view of the large number of magneto-optical experiments on InSb which have been reported so far, it is no longer appropriate simply to deduce a new set of band parameters from one set of data. In this contribution we present new intraband data for the conduction band as well as for the valence band at energies up to 130 meV. We attempt a unifying description of these results, high-field conduction-band cyclotron,¹ and combined resonance,² spin-flip data, and the interband data of Pidgeon and Brown³ (PB). A corrected form of the coupled-band scheme of PB is used.

A comprehensive analysis of the conduction band of InSb in magnetic fields up to 3.5 T was performed by Johnson and Dickey.⁴ They investigated the magnetotransmission in a conventional spectroscopic arrangement. Cyclotron resonance (CR) and impurity cyclotron resonance (ICR) were observed in samples with a carrier density $n_e \approx 10^{14} \text{ cm}^{-3}$. In higher-doped material ($n_e \approx 10^{15} \text{ cm}^{-3}$) also cyclotron resonance harmonics (CRH) were found with absorption coefficients up to 1 cm^{-1} . The results could be described in terms of a three-band model,⁵ where additionally the effect of remote bands was accounted for.⁴ According to Johnson and Dickey⁴ this nonparabolic theory gives magnetic energy levels correctly to energies as

high as 60 meV.

By a similar spectroscopic technique, magneto-absorption in fields up to 14 T was measured by Weiler *et al.*⁶ at energies between 80 and 160 meV. In view of interpreting the output behavior of the InSb spin-flip Raman laser highly doped samples with $n_e \approx 2 \times 10^{16} \text{ cm}^{-3}$ were used. For the same purpose another magneto-optical method was applied. Magnetotransmission of CO₂-laser light through highly doped *n*-InSb ($n_e > 10^{16} \text{ cm}^{-3}$) was studied by Dennis *et al.*^{7,8} and Favrot *et al.*⁹ The observed structure was interpreted in terms of Pidgeon-Brown model calculations.³ The agreement between experimental and theoretical resonant magnetic field values, however, turned out to be rather poor.^{8,6} There may be two reasons for this: on one hand, line broadening by nonparabolicity and the presence of impurities in highly doped material causes uncertainties in peak positions. On the other hand, the sets of band parameters used^{6,8} had been determined from interband magneto-optical experiments. No effort was undertaken to vary these parameters in order to obtain an optimum fit to the experimental intraband results.

Few experiments on magneto-optical transitions in the valence band have been reported so far.¹⁰⁻¹² The degeneracy of light- and heavy-hole bands at $k=0$ leads to the quantum effects described first

by Luttinger.¹³ The degeneracy results in nonuniform spacing of Landau ladders. Also some Landau levels in the immediate vicinity of the valence-band edge attain their maximum energy at $k_z \neq 0$. Earlier cyclotron-resonance experiments in the valence band of InSb met these specific difficulties in their interpretation.¹⁰⁻¹² One way to simplify somewhat the band structure is to apply uniaxial pressure, which lifts the valence-band degeneracy. The Landau ladders in an applied magnetic field then become more and more regular. A detailed investigation of hole cyclotron-resonance transitions was undertaken by Ranvaud.^{14,15} He was led to a set of band parameters for a Pidgeon-Brown treatment, which distinctly differs from that obtained by interband transitions. The photoconductivity technique was proven to be an excellent tool for detection of weak magneto-optical transitions. Kaplan¹⁶ has demonstrated that the spectral dependence of the photoconductivity matches that of the absorption constant for the fundamental impurity and electron cyclotron-resonance transitions.¹⁷

In this paper we report a systematic study of higher-order intraband transitions between Landau levels and energies in the range of 120 meV in magnetic fields up to 20 T. The magnetophotoconductivity induced by a CO₂ laser, operating at either 9.54, 10.26, or 10.59 μm , exhibits a number of sharp and well-resolved maxima in pure *n*- and *p*-type samples with carrier concentrations of some 10^{13} cm^{-3} . These are ascribed to different types of cyclotron-resonance harmonics. In *n*-type InSb with low carrier density, the free-electron transitions are well separated from the corresponding excitations of bound electron states. We have also observed a number of spin reversing transitions. LO-phonon-assisted cyclotron-resonance harmonic transition (LOCRH) were found both in the conduction and the valence bands.

Some of the free-electron transitions observed by us and other authors cannot be explained in terms of the selection rules given by Bell and Rogers,¹⁸ who did not account for the k_z -induced spin-flip excitations. In Sec. II we present main elements of the theory accounting for k_z terms, warping, and inversion asymmetry. Our results obtained for the [100] field orientation are in agreement with a recent treatment of Weiler *et al.*¹⁹ The transition energies for both electrons and holes are compared with theoretical predictions of the corrected Pidgeon-Brown model.³ It is shown that all observed transitions can be described with one single set of band parameters which also gives the correct energies for the earlier experimental interband data of Pidgeon and Brown.³

II. THEORY

We correct and extend the treatment of Pidgeon and Brown by taking into account the motion along the magnetic field (k_z terms) as well as the cubic nonsphericity and inversion asymmetry of the crystal. We consider the case of magnetic field parallel to the [100] crystallographic direction.

The initial Hamiltonian is given in the form of an 8×8 matrix, treating exactly the $\vec{k} \cdot \vec{p}$ interaction between Γ_6 , Γ_8 , and Γ_7 levels and incorporating other bands to the order of k^2 . We decompose the complete problem $D = D_0 + D_1$ into the part D_0 solvable in terms of a single column of harmonic oscillator functions (*s*) and $D_1 = D_w + D_k + D_G$, which accounts for warping (*w*), linear *k* terms (*k*), and the *G* terms (*G*). The last two contributions are due to the inversion asymmetry of InSb. In the basis used by Pidgeon and Brown the D_0 matrix has the form²⁰ shown in Table I, where $C = \hbar^2/m_0$, $s = eH/\hbar c$, $\gamma_1 = \gamma_1^L - 2P^2/3\epsilon_g$, Δ is the spin-orbit energy, and other parameters are defined according to Kane.²¹ a^\dagger and a are the creation and annihilation operators. The eigenvalue problem $D_0\Psi = E_0\Psi$ has the following solutions for the conduction band,

$$\Psi_{1N}^0 = \begin{bmatrix} A_{1N}^1 \Phi_N \\ a_{2N}^1 \Phi_{N-1} \\ a_{3N}^1 \Phi_{N+1} \\ a_{4N}^1 \Phi_{N+1} \\ 0 \\ a_{6N}^1(\zeta) \Phi_N \\ a_{7N}^1(\zeta) \Phi_{N+2} \\ a_{8N}^1(\zeta) \Phi_N \end{bmatrix}, \quad \Psi_{2N}^0 = \begin{bmatrix} 0 \\ a_{2N}^2(\zeta) \Phi_{N-2} \\ a_{3N}^2(\zeta) \Phi_N \\ a_{4N}^2(\zeta) \Phi_N \\ A_{5N}^2 \Phi_N \\ a_{6N}^2 \Phi_{N-1} \\ a_{7N}^2 \Phi_{N+1} \\ a_{8N}^2 \Phi_{N-1} \end{bmatrix}, \quad (1)$$

corresponding to the two projections of the total angular momentum $j_z = \pm \frac{1}{2}$ on the magnetic field direction (*b* and *a* sets, respectively). The big components in the wave functions are of the order $(A_\mu)^2 \simeq (\epsilon_g + \epsilon_\mu)/(\epsilon_g + 2\epsilon_\mu)$ and the small ones $(a_\mu)^2 \simeq \epsilon_\mu/(\epsilon_g + 2\epsilon_\mu)$ (cf. Zawadzki²²). We denote $\zeta = k_z(\hbar c/eH)^{1/2}$. The coefficients $a_\mu(\zeta)$ go to zero for $\zeta \rightarrow 0$. The above functions are taken as zero-order solutions.

In the same basis the D_1 matrix is shown in Table II, where $\Delta\gamma = \gamma_3 - \gamma_2$, while *K* and *G* are defined in Ref. 21. The terms corresponding to different peculiarities of the band structure can be easily identified. The D_1 matrix is treated as perturbation to the zero-order solutions (1). This completes the calculation of electron eigenstates. Due to the strong interband coupling all peculiarities

TABLE III. The $A_{\pm} = \partial D / \partial k_z$ matrix.

	Hermitian conjugate
$2C(F + \frac{1}{2})k_z$	
$-2iC\sqrt{s}Ga^\dagger$	$2C(\gamma_2 - \frac{1}{2}\gamma_1)k_z$
$i(2/\sqrt{3})C\sqrt{s}Ga$	$-2K$
$-2\sqrt{\frac{2}{3}}C\sqrt{s}Ga$	$i2\sqrt{2}C\gamma_2k_z$
0	0
$\sqrt{\frac{2}{3}}CP$	$(i/\sqrt{3})CP$
0	$2C(F + \frac{1}{2})k_z$
$-i\sqrt{6}C\sqrt{s}\gamma_3a^\dagger$	$-3C\sqrt{s}\gamma_3a$
0	0
$-i(\sqrt{3})CP$	$-i(2/\sqrt{3})C\sqrt{s}Ga^\dagger$
	$-2C(\gamma_2 + \frac{1}{2}\gamma_1)k_z$
	$2K$
	$2C(\gamma_2 - \frac{1}{2}\gamma_1)k_z$
	$-i\sqrt{2}C\gamma_2k_z$
	$-i\sqrt{2}K$
	$-C\gamma_2k_z$

TABLE IV. The $A_{\pm} = \partial D / \partial a$ matrix.

$Cs(2F + 1)a^\dagger$	$2iC\sqrt{s}Gk_z$	$i/\sqrt{3})C\sqrt{s}P$	0	$2\sqrt{\frac{2}{3}}CsGa$	0	$(2i/\sqrt{3})CsGa$
$-iC\sqrt{s}P$	$-Cs(\gamma_1 + \gamma_2)a^\dagger$	$-Cs\sqrt{3}(\gamma_2 + \gamma_3)a$	$i\sqrt{6}Cs(\gamma_2 + \gamma_3)a$	0	$i\sqrt{6}Cs\gamma_2k_z$	$i\sqrt{6}Cs\gamma_2k_z$
$(2i/\sqrt{3})C\sqrt{s}Gk_z$	$\sqrt{3}Cs\Delta\gamma a$	$-Cs(\gamma_1 - \gamma_2)a^\dagger$	$-Cs(\gamma_1 - \gamma_2)a^\dagger$	$-2\sqrt{\frac{2}{3}}CsGa$	$-i\sqrt{6}Cs\gamma_2k_z$	$-i\sqrt{6}Cs\gamma_2k_z$
$(-2\sqrt{2}/\sqrt{3})C\sqrt{s}Gk_z$	$2i\sqrt{\frac{3}{2}}Cs\Delta\gamma a$	$-i\sqrt{2}Cs\gamma_2a^\dagger$	$-Cs\gamma_2a^\dagger$	$(-2i/\sqrt{3})CsGa$	$\sqrt{3}CsK$	0
0	0	$2\sqrt{\frac{2}{3}}CsGa$	$(2i/\sqrt{3})CsGa$	$Cs(2F + 1)a^\dagger$	$(-2i/\sqrt{3})C\sqrt{s}Gk_z$	$2\sqrt{\frac{2}{3}}C\sqrt{s}Gk_z$
$-2\sqrt{\frac{2}{3}}CsGa$	$i\sqrt{2}CsK$	0	$-3C\sqrt{s}\gamma_2k_z$	$(-i/\sqrt{3})C\sqrt{s}P$	$-Cs(\gamma_1 - \gamma_2)a^\dagger$	$i\sqrt{2}Cs\gamma_2a^\dagger$
0	0	$i\sqrt{2}CsK$	$-i\sqrt{2}CsK$	$2iC\sqrt{s}Gk_z$	$\sqrt{3}Cs\Delta\gamma a$	$-i\sqrt{6}Cs\Delta\gamma a$
$(2i/\sqrt{3})CsGa$	$\sqrt{s}K$	$-3C\sqrt{s}\gamma_2k_z$	0	$\sqrt{\frac{2}{3}}C\sqrt{s}P$	$-i\sqrt{2}Cs\gamma_2a^\dagger$	$-Cs\gamma_2a^\dagger$

$\vec{E} \perp \vec{H}$. Polarization σ_L .

$$\Delta S=0. \quad \Delta N=+1 (s); -3, +5 (w); -1, +3 (\zeta k). \quad (2a)$$

$$\Delta S=-1. \quad \Delta N=+2 (\zeta); -2, +6 (w\zeta); \\ 0, +4 (k); -4, +8 (wk). \quad (2b)$$

$$\Delta S=+1. \quad \Delta N=0 (\zeta); \pm 4 (w\zeta); \pm 2 (k); \pm 6 (wk). \quad (2c)$$

$\vec{E} \perp \vec{H}$. Polarization σ_R .

$$\Delta S=0. \quad \Delta N=-1 (s); +3, -5 (w); +1, -3 (\zeta k). \quad (3a)$$

$$\Delta S=-1. \quad \Delta N=0 (\zeta); \mp 4 (w\zeta), \mp 2 (k); \mp 6 (wk). \quad (3b)$$

$$\Delta S=+1. \quad \Delta N=-2 (\zeta); +2, -6 (w\zeta); \\ 0, -4 (k); +4, -8 (wk). \quad (3c)$$

For example, $(w\zeta)$ means that the transition becomes allowed if warping and k_z terms are added to the spherical approximation. The G terms and linear k terms induce the same transitions.

Since, in the above formalism, the wave functions for all bands in question have the same form and the interaction Hamiltonian for interband and intraband transitions is the same, the selection rules for interband and intraband excitations in both bands are also identical.²⁵ However, it has been customary in the magneto-optical literature to use a somewhat different convention for interband transitions. It corresponds to increasing the numbers of the valence states by one, thus subtracting unity from all above ΔN . When describing the interband excitations with this prescription our results contain selection rules for spherical ($\Delta N = 0, -2$) and warping-induced ($\Delta N = +2, \pm 4, -6$) transitions, described and observed by Pidgeon and Brown. They are used later for the interpretation of their interband data.

III. EXPERIMENTAL

The experimental results were performed on InSb samples prepared from either n -type material with a free carrier concentration of $8 \times 10^{13} \text{ cm}^{-3}$ and a mobility of $4 \times 10^5 \text{ cm}^2/\text{V sec}$ at 77 K and p -type material with respective values of $1.6 \times 10^{13} \text{ cm}^{-3}$ and $8.5 \times 10^3 \text{ cm}^2/\text{V sec}$. They were cut along the [100], [110], or [111] axis and had typical dimensions $4 \times 5 \times 6 \text{ mm}^3$. These samples were cooled down to 8 K in the exchange gas chamber of a variable temperature gas-flow cryostat. The experiments were performed in the 5-cm bore of a 15- or a 20-T Bitter magnet. The magnetic

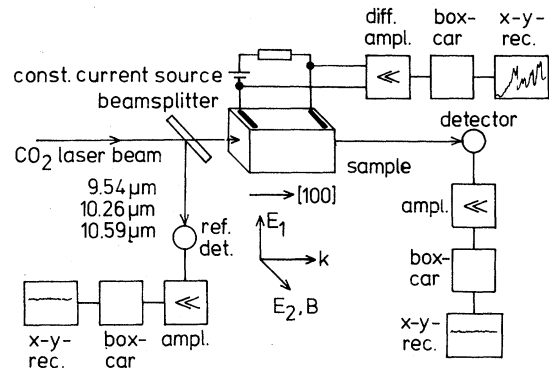


FIG. 1. Schematic experimental setup.

field \vec{H} was applied parallel to a [100], [110], or [111] crystallographic direction of the sample.

The experimental setup is schematically drawn in Fig. 1. As a light source we used a Q-switched CO₂ laser equipped with an intracavity grating to select the 9.54, 10.26, or 10.59- μm single lines. The maximum pulse peak power was 10 kW and the duration 300 nsec with a repetition rate of 150 sec^{-1} .

A small fraction of the incident laser light could be reflected onto a pyroelectric reference detector by means of a CdTe beam splitter. The remaining laser light traversed the sample in Voigt configuration with its electric vector either $\vec{E} \perp \vec{H}$ or $\vec{E} \parallel \vec{H}$. In some cases, the transmitted light was also monitored by means of a liquid-nitrogen cooled HgCdTe photoconductive detector. The signals were amplified, integrated by gated electronics and recorded as a function of magnetic field.

A constant current of 8–30 mA was applied to the sample by two soldered contacts. The corresponding dc voltage drop was fed into a fast differential amplifier (Tektronix 7A13), integrated by a boxcar system (PAR 160), and recorded versus magnetic field by an x - y recorder.

IV. RESULTS

Typical recorder tracings of the photoconductivity as a function of magnetic field obtained with n -type samples are shown in Figs. 2–5. In all cases, the laser reference signal displayed a negligible short-term instability of less than 3%. Figures 2(a), 2(b), and 2(c) gives a comparison of spectra for three different CO₂-laser wavelengths at fields up to 15 T, clearly demonstrating a shift of the resonant structure to lower fields with the wavelength proceeding to higher values. Figure 2(d) reproduces a transmission spectrum measured under the same experimental conditions as that of

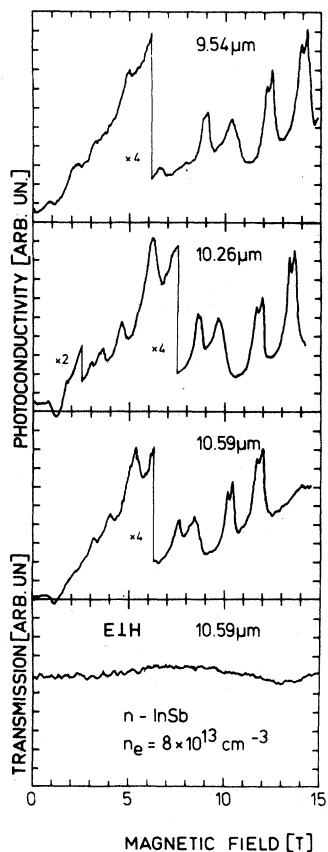


FIG. 2. (a), (b), and (c): Photoconductive spectra taken in n -InSb at three different CO_2 -laser wavelengths ($\vec{E} \perp \vec{H}$, $T \approx 12$ K); (d): Transmission spectrum taken simultaneously with (c).

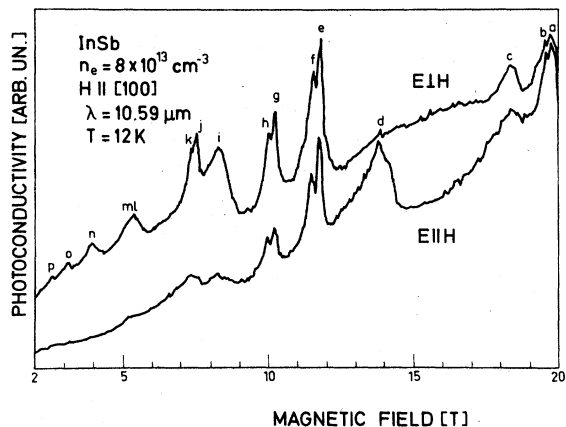


FIG. 3. Photoconductive spectra of n -InSb for $\vec{H} \parallel [100]$ ($\lambda = 10.59 \mu\text{m}$, $T \approx 12$ K).

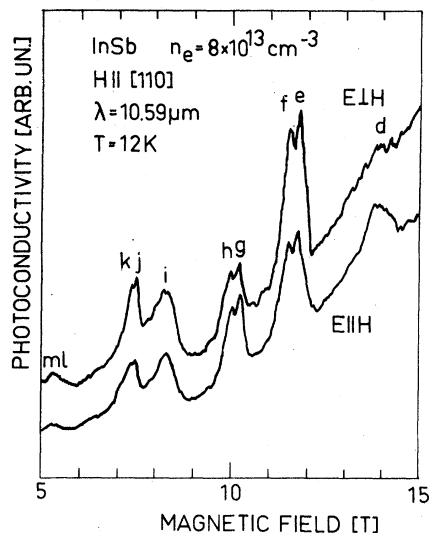


FIG. 4. Photoconductive spectra of n -InSb for $\vec{H} \parallel [110]$ ($\lambda = 10.59 \mu\text{m}$, $T \approx 12$ K).

the photoconductivity in Fig. 2(c). Due to the small absorption constant (of the order of 10^{-2} cm^{-1}) for our low-carrier concentrations the transmission spectrum does not exhibit any distinct structure. The striking gain in sensitivity due to application of the photoconductivity technique is evident.

Photoconductive spectra taken on n -type InSb at $10.59 \mu\text{m}$ for $\vec{H} \parallel [100]$ for both polarizations $\vec{E} \parallel \vec{H}$ and $\vec{E} \perp \vec{H}$ are plotted in Fig. 3. The corresponding recordings for $\vec{H} \parallel [110]$ and $\vec{H} \parallel [111]$ are shown in Figs. 4 and 5.

The spectra obtained with p -type material (Fig. 6) also exhibits a distinct structure which consist-

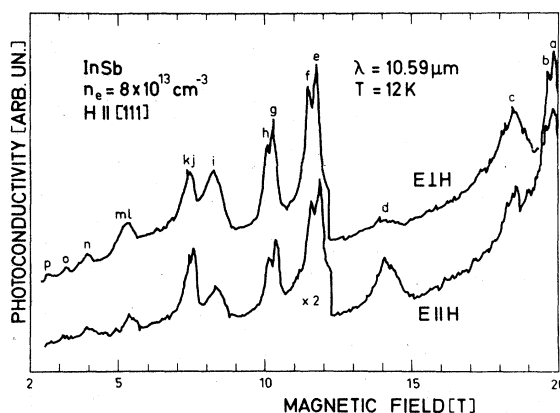


FIG. 5. Photoconductive spectra of n -InSb for $\vec{H} \parallel [111]$ ($\lambda = 10.59 \mu\text{m}$, $T \approx 12$ K).

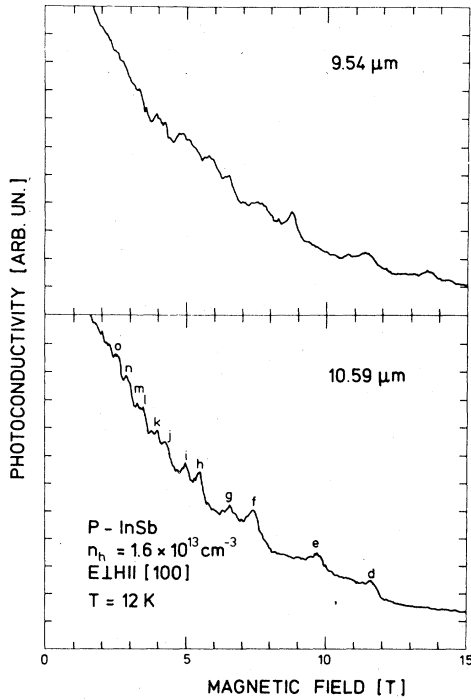


FIG. 6. Photoconductive spectra of p -InSb for $\vec{H} \parallel [100]$ ($\vec{E} \perp \vec{H}$, $T \approx 12$ K).

TABLE VI. Resonant magnetic field values for p -type InSb ($\vec{H} \parallel [100]$).

Peak ^a	Assignment	H (T) for wavelength	
		9.54 μm	10.59 μm
<i>d</i>	$[b^+(0) - b^+(2)]^*$	13.60	11.60
<i>e</i>	$[a^+(0) - a^+(3)]^*$	11.45	9.65
<i>f</i>	$[b^+(0) - b^+(3)]^*$	8.75	7.38
<i>g</i>	$[a^+(0) - a^+(4)]^*$	7.60	6.55
<i>h</i>	$[b^+(0) - b^+(4)]^*$	6.45	5.45
<i>i</i>	$[a^+(0) - a^+(5)]^*$	5.82	5.00
<i>j</i>	$[b^+(0) - b^+(5)]^*$	5.05	4.27
<i>k</i>	$[a^+(0) - a^+(6)]^*$	4.70	3.96
<i>l</i>	$[b^+(0) - b^+(6)]^*$	4.20	3.50
<i>m</i>	$[a^+(0) - a^+(7)]^*$	3.85	3.26
<i>n</i>	$[b^+(0) - b^+(7)]^*$	3.57	2.85
<i>o</i>	$[a^+(0) - a^+(8)]^*$	3.35	2.60

^a The letters refer to Fig. 6.

ently shifts to higher magnetic fields as the incident wavelength is reduced from 10.59 to 9.54 μm . Since no distinct dependence on the polarization was observed, only the case of $\vec{E} \perp \vec{H}$ is plotted. Tables V and VI summarize the magnetic field values corresponding to peaks of the photoconductivity signal in the $H \parallel [100]$ geometry for n - and p -type InSb.

V. DISCUSSION

A. Remarks on the experimental conditions

The carrier density of $8 \times 10^{13} \text{ cm}^{-3}$ in the n -type samples corresponds to a Fermi energy of 0.5 meV ($H=0$). The ultraquantum limit is consequently reached already at ≈ 0.2 T. In all cases discussed below we are well above this field limit. Even at low finite lattice temperatures only states in the lowest Landau level $a^c(0)$ and the associated impurity levels are populated. These are the only possible initial states for intra-conduction-band transitions. In the p -type samples we do not reach this quantum limit because of the small Landau-level spacing of heavy holes near the band edge. In pure n -type InSb, magnetic freeze-out effects occur at high magnetic fields.²⁶ According to the calculations by von Ortenberg²⁷ the ratio between the occupations n_D of the impurity ground state, and n_e of the Landau level can be estimated. For a temperature of 15 K magnetic fields of even 20 T are not sufficient to depopulate the Landau state by more than about 50% (compensation ratio $K = N_A/N_D \approx 0.7$ for our n -type samples, N_A : acceptor concentration, N_D : donor concentration).

The highest applied current of 30 mA corresponds to a maximum electric field of some 100

TABLE V. Resonant magnetic field values for n -type InSb ($\vec{H} \parallel [100]$).

Peak ^a	Assignment	H (T) for wavelength		
		9.54 μm	10.26 μm	10.59 μm
<i>a</i>	$a^c(0) - b^c(1)$			19.85
<i>b</i>	$(000)a^c - (1M\lambda)b^c$			19.65
<i>c</i>	$[a^c(0) - a^c(1)]^*$		19.45	18.40
<i>d</i>	$[a^c(0) - b^c(1)]^*$	16.90	14.60	13.80
<i>e</i>	$a^c(0) - a^c(2)$	13.75	12.27	11.75
<i>f</i>	$(000)a^c - (2M\lambda)a^c$	13.45	12.00	11.50
<i>g</i>	$a^c(0) - b^c(2)$	12.10	10.65	10.20
<i>h</i>	$(000)a^c - (2M\lambda)b^c$	11.75	10.41	9.98
<i>i</i>	$[a^c(0) - a^c(2)]^*$	9.95	8.70	8.25
<i>j</i>	$a^c(0) - a^c(3)$	8.73	7.78	7.47
<i>k</i>	$(000)a^c - (3M\lambda)a^c$	8.55	7.62	7.32
<i>l</i>	$[a^c(0) - a^c(3)]^*$	6.35	5.53	5.32
<i>m</i>	$a^c(0) - a^c(4)$			
<i>n</i>	$[a^c(0) - a^c(4)]^*$	4.72	4.12	3.93
<i>o</i>	$[a^c(0) - a^c(5)]^*$	3.70	3.24	3.08
<i>p</i>	$[a^c(0) - a^c(6)]^*$	3.05	2.68	2.58

^a The letters refer to Figs. 3–5. The notation $(NM\lambda)$ for the impurity levels refers to N : Landau quantum number, M : z component of angular momentum, λ : number of nodes of wave function in z direction.

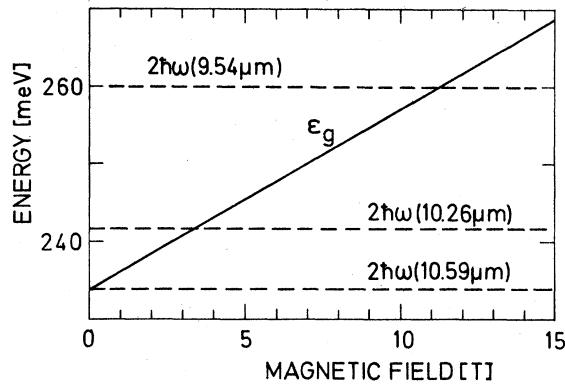


FIG. 7. Comparison of two-photon energies of CO_2 -laser lines used in this work and the band-edge energy of InSb vs magnetic field.

mV/cm at 20 T. Thus we are still in the Ohmic region of the current density electric field characteristics in high magnetic fields.²⁸ This was also verified by reducing the current to 8 mA, which did not affect the shape of the photoconductive spectra.

In order to avoid misinterpretations of the data, it is important to distinguish clearly between one-photon intraband and two-photon interband processes. The latter have been investigated in nearly identical arrangements,^{29,30} leading to spectra of a rather involved structure with a number of less distinct peaks than those observed in our case. For a clear distinction, we compare the two-photon energies of the three CO_2 -laser lines with the gap of forbidden energies in InSb increasing as a function of magnetic field (Fig. 7). The two-photon energy, corresponding to $\lambda = 10.59 \mu\text{m}$, is below the band edge for all magnetic fields. The resonant structure in the magnetophotoconductivity obtained at this wavelength in n -type material has a characteristic shape (see Fig. 2). The same structure can be identified for the wavelengths of 10.26 and 9.54 μm [Figs. 2(b) and 2(c)], a possible two-photon background clearly not interfering. A supplementary test was performed to exclude this possible background. The incident laser intensity was continuously attenuated by means of a variable-pressure ether cell down to $\frac{1}{10}$ of its original value. No change in the shape of the spectra was found. A two-photon contribution would have exhibited a square-law dependence on the light intensity. The same arguments hold for the case of p -type InSb (Fig. 6). The peaks assigned in Figs. 3–6 are thus unambiguously identified as originating from one-photon intraband transitions.

Whereas the photoconductivity technique is an excellent tool for the determination of transition

energies,^{17,31} the amplitudes of the photoconductivity peaks are not directly related to the absolute values of the absorption constant. Although the origin of the photoconductive response is the absorption process, its magnitude is related to a quantum transport phenomenon. Thus it depends also on the dominating scattering processes, which vary with temperature and energy. In fact mostly the carriers which are not in thermal equilibrium with the lattice are responsible for the observed photoconductive signal. In practice we have found that relative amplitudes of adjacent peaks depend somewhat on the direction of the applied dc electric field with respect to \vec{H} .

B. Cyclotron-resonance harmonic (CRH) transitions in n -type InSb

The peaks labelled a , e , g , and j in Figs. 3–5 are identified as free-electron transitions $a^c(0) - b^c(1)$, $a^c(0) - a^c(2)$, $a^c(0) - b^c(2)$, and $a^c(0) - a^c(3)$. Two different models were used for a comparison of the experimental data with the theory, the Johnson-Dickey (JD) model,⁴ which is an extension of the Bowers-Yafet treatment,⁵ and the corrected Pidgeon-Brown model³ (see Sec. II). The latter has been mainly used until now for the interpretation of interband transitions.

The parameters m_c^* and g_c^* used by JD (see Table VII) were obtained by fitting experimental data for energies below 18 meV. The calculated conduction-band energies agreed within 2% with experimental values up to 60 meV at fields below 3.5 T.⁴ Extending the calculation of Landau levels to higher energies and fields we found an increasing disagreement with the experimental data of ours as well as those of McCombe on cyclotron and combined resonance.^{1,2} We performed the calculations according to JD for various m_c^* and g_c^* without improving the fit. Thus we carried out the description of the available experimental data using a more complete Pidgeon and Brown (PB) treatment. A comparison of these data with transition energies calculated with the corrected PB scheme (see Sec. II) for $\vec{H} \parallel [100]$ is given in Fig. 8. The parameters for this calculation are listed in Table VII. For the spin-orbit splitting we use a value of 0.803 eV,^{32,33} rather than 0.9 eV as in the original Pidgeon-Brown treatment. E_p and γ^L were varied to give an optimum fit to both intra- and interband experimental data.

Also included in Fig. 8 are data on combined resonance $a^c(0) - b^c(1)$ and cyclotron resonance $a^c(0) - a^c(1)$,^{1,2} as well as spin-flip transition energies $a^c(0) - b^c(0)$ as deduced from the frequency of stimulated spin-flip Raman (SFR) scattering.⁴⁷ Even more precise values for the $a^c(0) - b^c(0)$

TABLE VII. Conduction-band parameters of InSb from various experiments.

Parameter	Interband MO	Intraband MO	This work
ϵ_g (eV)	0.23 ^a 0.2355 ^b 0.2367 ^c		0.2355
m_c^*/m	0.0145 ^{d,b} 0.0149 ^e 0.0139 ^g	0.013 ^h 0.0155 ⁱ 0.0145 ^j 0.0137 ^k 0.0139 ^l	0.0146
g_c^*	-48 ^{b,d} -47 ^m	-48 ⁿ -52 ⁱ -51.3 ^{o,1} -51.0 ^p	-47.8
E_p (eV)	21.92 ^b 23.71 ^g 21.21 ^e	21.21 ^j 24 ^l 24.4 ^t	21.6
Δ (eV)	0.9 ^b 0.81 ^f 0.803 ^q	0.81 ^l	0.803
γ_1^L	36 ^d 32.5 ^b 33.51 ^e	43.3 ^r 39.7 ^s	31.1
γ_2^L	14.5 ^d 14.3 ^b 14.48 ^e	19.7 ^r 18.1 ^s	14.3
γ_3^L	16.2 ^d 15.4 ^b 15.65 ^e	21.1 ^r 19.5 ^s	15.4
κ^L	13.4 ^b 13.47 ^e	17.5 ^r 17.4 ^s	13.9
q^L	0.39 ^e	0.4 ^{r,s}	0
F	0 ^b	0 ^{i,j}	0

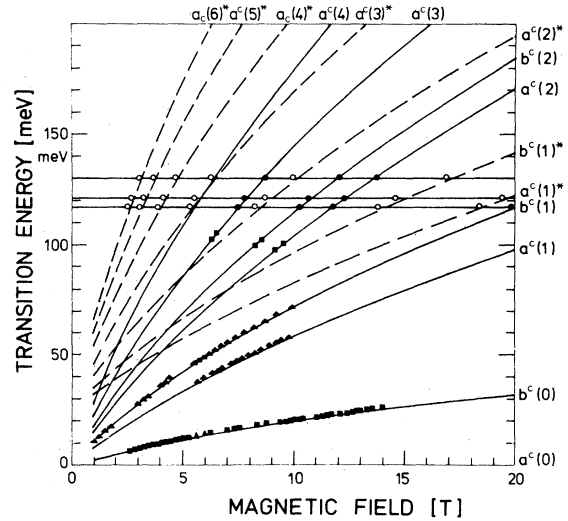
^a Roberts and Quarrington (Ref. 34).^b Pidgeon and Brown (Ref. 3).^c Johnson (Ref. 35).^d Zwerdling *et al.* (Ref. 36).^e Pidgeon and Groves (Ref. 37).^f Pidgeon *et al.* (Ref. 32).^g Bell and Rogers (Ref. 18).^h Dresselhaus *et al.* (Ref. 38).ⁱ Lax *et al.* (Ref. 39).^j Palik *et al.* (Ref. 40).^k Dennis (Ref. 41).^l Johnson and Dickey (Ref. 4).^m Pidgeon *et al.* (Ref. 42).ⁿ Bell (Ref. 43).^o Isaacson (Ref. 44).^p Konopka (Ref. 45).^q Aggarwal (Ref. 33).^r Ranvaud (Ref. 14).^s Ranvaud *et al.* (Ref. 15).^t Herman *et al.* (Ref. 46).

FIG. 8. Intraband transition energies. Straight line: free-electron transitions calculated from the corrected Pidgeon and Brown model; Dotted line: LO-phonon-assisted transitions, calculated from the same model; experimental values: ● free-electron transitions (this work); ○ LO-phonon-assisted transitions; ▲ cyclotron resonance, combined resonance and EDE-ESR data (Ref. 1); ■ spin-flip Raman data (Ref. 47).

transitions were obtained by electric-dipole-excited electron-spin-resonance (EDE-ESR) experiments.⁴⁸ Within the scale of Fig. 8, these values in the magnetic field range from 2.8 to 7.5 T do not differ from the SFR results. Extrapolating the corresponding g_c^* values to zero field from these data alone would yield a higher value than quoted in Table VII. Certain higher-order transition energies deduced from dips in the Stokes output of the SFR laser are also drawn.⁴⁷ All of these data are described within 2 meV by the calculated magnetic energy levels.

In Table VII we also give a collection of band parameters deduced from various intra- and interband magneto-optical (MO) investigations. A comparison of parameters obtained by different band models is not unambiguous. For example, Herman *et al.*⁴⁶ have recently interpreted intraband data in the parabolic region of energies by means of a model which explicitly accounts for the higher conduction bands Γ_7^c and Γ_8^c . In conjunction with obvious discrepancies in g_c^* values, McCombe¹ noted that corrections due to higher bands may become less important at low fields, i.e., calculations have weighted the higher band interactions too heavily at low fields. Therefore it might not be astonishing, that the value of $g_c^* = -47.8$ is different from the experimental values obtained at low magnetic fields.^{44,48}

As far as selection rules for conduction band transitions in the $\vec{H} \parallel [100]$ geometry are concerned, the transitions $a^c(0) - b^c(2)$ and $a^c(0) - a^c(3)$ (g and j in Fig. 3) are weaker for the $\vec{E} \parallel \vec{H}$ configuration than for $\vec{E} \perp \vec{H}$, and the $a^c(0) - b^c(1)$ transition d is weaker for $\vec{E} \perp \vec{H}$. This is in agreement with the selection rules given in Sec. II. Selection rules for samples oriented in other symmetry directions were given by Weiler *et al.*¹⁹ For the $\vec{H} \parallel [110]$ configuration (Fig. 4) we note that the $a^c(0) - a^c(2)$ and $a^c(0) - a^c(3)$ transitions (e and j) are stronger for $\vec{E} \perp \vec{H}$, whereas $a^c(0) - b^c(2)$ resonance (g) is stronger for $\vec{E} \parallel \vec{H}$, in agreement with theoretical predictions of Weiler *et al.* Agreement is also found for $\vec{H} \parallel [111]$ (Fig. 5). The transitions $a^c(0) - a^c(2)$ and $a^c(0) - b^c(2)$ (e and g in Fig. 5) are weaker for $\vec{E} \parallel \vec{H}$ and the $a^c(0) - a^c(3)$ transition (j) is weaker for $\vec{E} \perp \vec{H}$.

Several authors have observed relatively strong absorption peaks at magnetic fields corresponding to CRH transitions in InSb with $n_e \geq 10^{15} \text{ cm}^{-3}$.^{4,6,9,49,50} Weiler *et al.*¹⁹ have interpreted these transitions as originating from peculiarities of the InSb band structure. McCombe *et al.*⁵⁰ explained these transitions as involving plasmon emission⁵¹ and therefore rather independent of the orientation of H with respect to the crystallographic axis. Mycielski *et al.*⁵² suggested a mechanism based on electron-impurity interaction (see also Ref. 53).

It seems that also experimentally different observations have been made: whereas Favrot

*et al.*⁹ found a dependence of the selection rules for CRH on crystallographic orientation (using a cold finger technique for cooling the samples) McCombe⁵⁴ did not find such a dependence in absorption measurements, keeping the samples at 4.2 K.

Preliminary investigations of the photoconductivity as a function of temperature up to 65 K indicate that the difference in the spectral response for $\vec{E} \parallel \vec{H}$ and $\vec{E} \perp \vec{H}$ in the Voigt configuration becomes more pronounced and reflects better the selection rules given in Sec. II for most of the transitions.

From all these observations one might speculate that at low temperatures CRH transitions are also induced by electron-impurity or electron-plasmon interactions. With increasing lattice temperature, when these interactions are weaker, the available experimental data seem to indicate that then symmetry induced transitions become more and more important.

C. Impurity-cyclotron-resonance-harmonic (ICRH) transitions in n -type InSb

Some of the observed peaks (Figs. 2–5) exhibit a well-resolved splitting similar to that found in fundamental cyclotron resonance (CR) in pure samples.⁴ In order to identify its origin, photoconductive spectra were recorded at different temperatures (Fig. 9). In the same manner as for fundamental CR,⁴ the strength of the low-field component increases with respect to that of the high-field component as the temperature is decreased. This behavior indicates magnetic freeze-out effects, which occur when free electrons become more and more localized to donor sites at low temperatures and high magnetic fields. Actually, Fig. 9 is an excellent illustration of this phenomenon. The peaks labelled b, f, h, k in Figs. 3–5 are consequently assigned to impurity transitions.

Whereas the fundamental ICR transition has been investigated up to fields of 10 T by Kaplan,¹⁷ no experimental information on ICRH transitions has been available until now, for the simple reason, that CRH resonances $a^c(0) - a^c(N)$, $b^c(N)$ for $N \geq 2$ are very weak. Carrier concentrations of at least 10^{15} cm^{-3} are required to observe distinct changes in transmission. With such a number of impurities, the bound-electron wave functions overlap with one another, forming a tail of the Landau density of states which hampers the observation of impurity transitions. In contrast to that, the photoconductivity technique is suitable for the investigation of pure samples, with appreciable changes in the electric signal for weak transitions, also between bound states.³¹

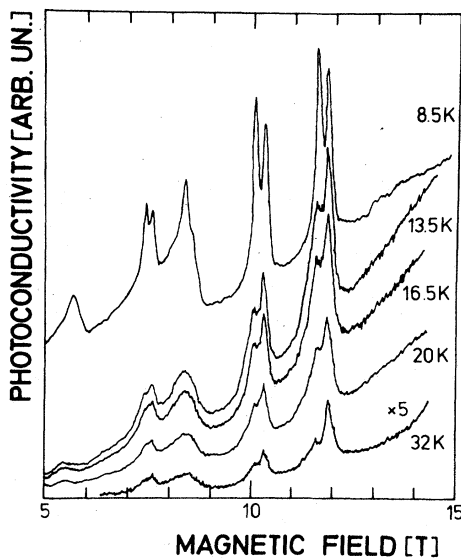


FIG. 9. Photoconductive spectra taken at various lattice temperatures ($\vec{E} \perp \vec{H}$, $\lambda = 10.59 \mu\text{m}$).

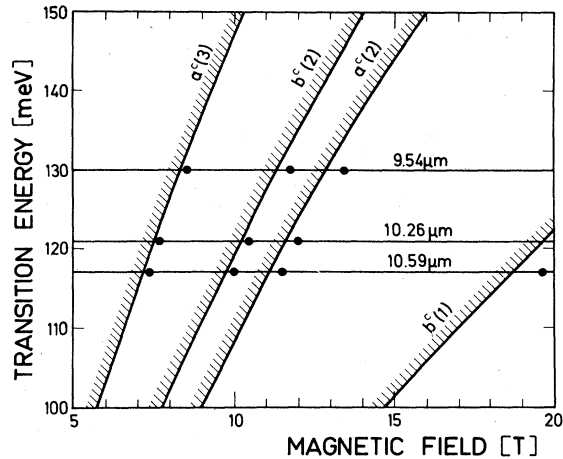


FIG. 10. Impurity transition energies vs magnetic field with the experimental $(000)a^c$ energy (Ref. 26) as zero point (dots). Landau level energies are given in the same normalization.

It is evident that we observe transitions between the impurity ground state $(000)a^c$ and impurity states associated with either the $a^c(N)$ or $b^c(N)$ sets of free-electron magnetic energy levels. A detailed interpretation is in progress, treating the observed impurity transitions in a model that is consistent with the description of Landau levels in Sec. II.

In Fig. 10 we have plotted the impurity transition energies versus magnetic field, counted from the experimental $(000)a^c$ energy as determined by Neuringer.²⁶ Corresponding Landau levels are drawn in the same energy scale.

D. LO-phonon-assisted cyclotron resonance harmonics (LOCRH) transitions in *n*-type InSb

Another series of peaks in Figs. 2–5 is interpreted as LO-phonon-assisted cyclotron harmonic transitions $[a^c(0) - a^c(N)]^*$: These resonances are well known and have been investigated in lower magnetic fields both experimentally^{49,55,56} and theoretically.^{49,57} We calculated the transition energies (dashed lines in Fig. 8) using an LO-phonon energy of 24.6 meV, as deduced from a far infrared reflection measurement at 4.2 K. Experimental values are drawn by open circles in Fig. 8. All transitions are found at somewhat higher energies than expected theoretically. This is in qualitative agreement with an inhomogeneous broadening mechanism suggested by Morita *et al.*⁵⁵ who considered the effect of LO phonons with wave vector $q \neq 0$. The shift, according to Morita *et al.*, is expected to be $\Gamma/\sqrt{3}$, where Γ is a damping con-

stant. We can estimate Γ from the width of free electron transitions to be roughly 2.5 meV for intermediate fields. The shift of the LO-phonon resonance should then be ≈ 1.5 meV, which is somewhat less than we observe (Fig. 8). Morita *et al.*⁵⁵ also remarked, that no LOCRH transitions could be observed in very pure samples. This might suggest that impurities are involved in the phonon resonances. Impurity states were recently reported to affect magneto-optical spectra of *n*-InSb at magnetic fields where the transition energies $a^c(0) - a^c(2) \approx [a^c(0) - a^c(1)]^*$.⁵⁸ Possible similar effects on other transitions should be carefully investigated.

Selection rules for spin-conserving LOCRH resonances in the conducting band of InSb were deduced from a theory for parabolic bands by Enck *et al.*⁴⁹ who predicted resonant transitions for $\Delta N = 1, 2, 3, 4, \dots$ in the $\vec{E} \perp \vec{H}$ polarization and non-resonant behavior for $\vec{E} \parallel \vec{H}$. The latter conclusion is a direct consequence of the k_z dependence of the matrix element for the radiation part of the transition. All corrections to the band structure (spin-orbit interaction, warping, inversion asymmetry) which lead to additional transitions at $k_z \neq 0$ for $\vec{E} \parallel \vec{H}$, may lead to weakly allowed phonon-assisted resonances also for the $\vec{E} \parallel \vec{H}$ polarization. We actually observe these transitions for the parallel polarization (Figs. 3–5).

The transition $[a^c(0) - b^c(1)]^*$, involving a phonon-assisted spin-flip, has been treated theoretically by Zawadzki,⁵⁹ including explicitly the interband $\vec{k} \cdot \vec{p}$ coupling and the spin-orbit interaction. That theory predicts a strong resonance for $\vec{E} \parallel \vec{H}$ and a weak resonance for $\vec{E} \perp \vec{H}$. This is confirmed experimentally by the intensities of the peak labelled *d* in Figs. 3–5.

E. LO-phonon-assisted cyclotron resonance harmonic (LOCRH) transitions in *p*-type InSb

Very few magneto-optical experiments in the valence band of InSb have been reported so far. Apart from experimental difficulties due to low-hole mobilities of the order of some 1000 cm²/V sec, there are some theoretical problems with exact interpretation of results. Hensel and Suzuki²⁴ showed that the degeneracy of the valence bands at the center of the Brillouin-zone causes most experimentally observable intraband transitions in the vicinity of the band edge to take place at points other than $k_z = 0$. The calculation of these k_z -dependent energy differences is quite complicated and the interpretation of the early cyclotron-resonance experiments performed in the microwave and millimeter region^{10–12} suffered from this fact.

An appreciable simplification of this complication

in the band structure can be obtained by the application of uniaxial stress. This destroys the cubic symmetry which is responsible for the degeneracy of the valence bands. In the limit of high stress, the observed transitions take place at $k_z=0$. Ranvaud *et al.*^{14,15} investigated different magneto-optical transitions as a function of applied stress using a HCN laser source with a quantum energy of 3.68 meV. Extrapolating to zero stress then gives the $k_z=0$ transition energies. He was thus able to derive a set of band parameters for the Pidgeon-Brown coupled band scheme which describes Landau-level energies within a few meV near the valence-band edge. These parameters, however, are about 30% larger than those obtained from interband transitions (see Table VII).

One of the major shortcomings of optical experiments with the HCN laser is its small quantum energy, allowing one to observe only transitions very near to the band edge, where the described difficulties are most pronounced. The CO₂ laser, on the other hand, with its high quantum energy of about 120 meV, does induce transitions of holes with final states deep in the band. In contrast to the *n*-type material even at highest magnetic fields several Landau levels are thermally populated in our *p*-type material. Amongst these are not only heavy-hole states $a^-(N)$ and $b^-(N)$, but also the lowest quantum number light-hole states $a^+(0)$ and $b^+(0)$. The latter, due to Luttinger effects, are

split by less than 2 meV from the band-edge state $b^-(0)$ for the whole field range in question. The photoconductivity peaks in Fig. 6 are thus likely to arise from light holes, the heavy-hole states being so closely spaced that different transitions cannot be resolved.

Within the framework of the same corrected PB treatment we can assign the resonances shown in Fig. 6 to the LO-phonon assisted light-hole transitions $[a^+(0) - a^+(N)]^*$ and $[b^+(0) - b^+(N)]^*$ (Fig. 11). The same band parameters as given in Table VII were used in calculating valence-band Landau levels and corresponding transition energies. Experimental values agree within 3 meV with the theoretical ones, which seems satisfactory.

The light-hole transitions $a^+(2) - a^+(3)$ and $b^+(0) - b^+(1)$, as observed by Ranvaud,^{14,15} agree within 0.3 meV with our calculated Landau-level energies. The transition $a^+(0) - a^+(1)$, however, deviates by about 0.8 meV from this scheme.

F. Interband magneto-optical transitions

Since the magneto-optical interband transitions in InSb have been first described in terms of a coupled band scheme by Pidgeon and Brown³ the question has been frequently risen, why intraband transitions could not be described by the same parameters.

In Figs. 12 and 13 we compare the interband ex-

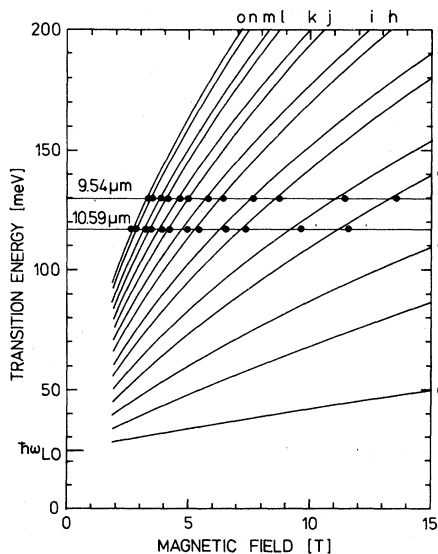


FIG. 11. LO-phonon-assisted light-hole-transition energies. Straight line: calculated from the corrected Pidgeon-Brown model; ● experimental values. Labels refer to Table VI.

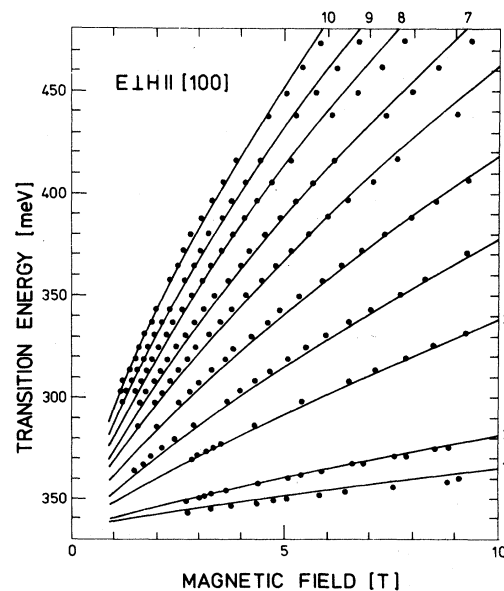


FIG. 12. Interband transition energies for $\vec{E} \perp \vec{H} \parallel [100]$; Straight line: calculated from the corrected Pidgeon-Brown model; ● experimental values of Pidgeon and Brown (Ref. 3). Notation as in Ref. 3.

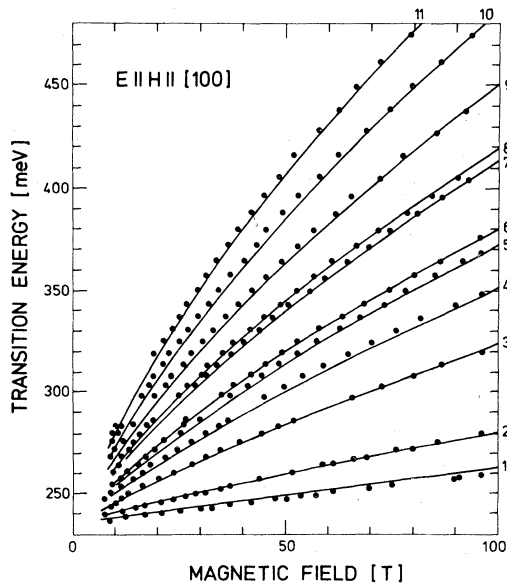


FIG. 13. As Fig. 12, but $\vec{E} \parallel \vec{H} \parallel [100]$.

perimental results of Pidgeon and Brown³ with our calculated transition energies. The same set of band parameters as for conduction and valence-band transitions was used (see Table VII). The agreement is in general as good as in the original fit of Pidgeon and Brown and should be regarded as satisfactory. Small deviations occur in the lowest energy transitions for both polarizations, involving the $a^-(2)$ and $b^-(2)$ levels, respectively.

VI. CONCLUSIONS

Photoconductivity experiments on pure semiconductors in high magnetic fields provide a very effective tool in the investigations of different magneto-optical transitions. For a precise determination of peak positions due to higher-order transitions, photoconductivity is clearly superior to transmission spectroscopy, since material with very low carrier densities can be investigated. Amplitudes of photoconductive spectra, however,

are not simply proportional to the transition strengths.

Magneto-optical intraband excitations at relatively high energies of about 120 meV have been observed both in the conduction and in the valence band of InSb at fields up to 20 T. A description is given in terms of a corrected Pidgeon-Brown model. Optical selection rules for free-electron transitions were derived from a scheme where the interaction Hamiltonian $H' = (e/c)\vec{A} \cdot \vec{v}$ is used in a matrix representation and therefore differs substantially from the scalar form of interaction. Most of the observed free-electron transitions are accounted for by this theory. Some resonances, however, remain unexplained. The even CRH transitions $\vec{E} \perp \vec{H}$, in particular the $a^c(0) - a^c(2)$ resonance, reported by various authors, could be interpreted in terms of impurity-assisted excitations.^{53,60} LO-phonon assisted transitions were observed in the conduction band and, for the first time, in the valence band of InSb. All these excitations, including cyclotron harmonics in the conduction band, are described by the corrected Pidgeon-Brown model with a single set of band parameters. The earlier experimental interband data of Pidgeon and Brown are also in good agreement with this scheme. Thus, for the first time a unified description of magneto-optical inter- and intraband transitions in InSb is achieved, providing the most demanding verification of a band structure calculation for a small-gap semiconductor.

ACKNOWLEDGMENT

This work was supported by the Stiftung Volkswagenwerk. One of us (G.B.) would like to thank the Deutsche Forschungsgemeinschaft for a grant of travel expenses. We thank Professor K. Dransfeld for his interest in this work. It is a pleasure to acknowledge the continuous helpful experimental assistance of Mr. M. Berger and, in part of the experiments of Mr. S. Hayashi. We are very grateful to Drs. R. Ranvaud, P. Vogl, and H.-R. Trebin for valuable discussions. We thank Dr. Margaret H. Weiler for sending us a preliminary version of her paper prior to publication.

*Present address: AEG Telefunken Forschungsinstitut, Goldsteinstr. 235, 6000 Frankfurt-Niederrad, FRG.

†Present address: Chromatix GmbH, Unter Strasse 45a, 6903 Neckargemünd, FRG.

¹B. D. McCombe, Phys. Rev. **181**, 1206 (1969).

²B. D. McCombe, S. G. Bishop, and R. Kaplan, Phys. Rev. Lett. **18**, 748 (1967).

³C. R. Pidgeon and R. N. Brown, Phys. Rev. **146**, 575 (1966).

⁴E. J. Johnson and D. H. Dickey, Phys. Rev. B **1**, 2676 (1969).

⁵R. Bowers and Y. Yafet, Phys. Rev. **115**, 1165 (1959).

⁶M. H. Weiler, R. L. Aggarwal, and B. Lax, Solid State Commun. **14**, 299 (1974).

⁷R. B. Dennis, R. A. Wood, C. R. Pidgeon, S. D. Smith, and J. W. Smith, J. Phys. C **5**, L73 (1972).

⁸R. B. Dennis, C. R. Pidgeon, S. D. Smith, B. S. Wherret, and R. A. Wood, Proc. R. Soc. Lond.

- A 331, 203 (1972).
- ⁹G. Favrot, R. L. Aggarwal, and B. Lax, *Solid State Commun.* **18**, 577 (1976); in *Proceedings of the Third International Conference on Light Scattering in Solids, Campinas, 1975*, edited by M. Balkanski (Flammari-
on, Paris, 1976), p. 286; in "Proceedings of the International Conference on Magneto-Optics, Zurich, 1976," *Physica* **89B**, 218 (1977).
- ¹⁰D. M. S. Bagguley, M. L. A. Robinson, and R. A. Stradling, *Phys. Lett.* **6**, 143 (1963).
- ¹¹M. L. A. Robinson, *Phys. Rev. Lett.* **17**, 963 (1966).
- ¹²K. J. Button, B. Lax, and C. C. Bradley, *Phys. Rev. Lett.* **21**, 350 (1968).
- ¹³J. M. Luttinger, *Phys. Rev.* **102**, 1030 (1956).
- ¹⁴R. Ranvaud, Ph.D. thesis (Brown University, 1973) (unpublished).
- ¹⁵R. Ranvaud, F.H. Pollak, U. Rössler, and H.-R. Trebin, in *Proceedings of the Thirteenth International Conference on the Physics of Semiconductors, Rome, 1976*, edited by F. G. Fumi (Tipografia, Marves, Rome, 1976), p. 1171.
- ¹⁶R. Kaplan, *Appl. Opt.* **6**, 685 (1967).
- ¹⁷R. Kaplan, *Phys. Rev.* **181**, 1154 (1969).
- ¹⁸R. L. Bell and K. T. Rogers, *Phys. Rev.* **152**, 746 (1966).
- ¹⁹M. H. Weiler, R. L. Aggarwal, and B. Lax, *Phys. Rev. B* **17**, 3269 (1978).
- ²⁰This form corrects a few small errors made by Pidgeon and Brown.
- ²¹E. O. Kane, *J. Phys. Chem. Solids* **1**, 249 (1957).
- ²²W. Zawadzki, in *New Developments in Semiconductors*, edited by P. R. Wallace (Leyden, 1973), p. 441.
- ²³J. J. Stickler, H. J. Zeiger, and G. S. Heller, *Phys. Rev.* **127**, 1077 (1962).
- ²⁴K. Suzuki, and J. C. Hensel, *Phys. Rev. B* **9**, 4184 (1974); J. C. Hensel, and K. Suzuki, *ibid.* **4219** (1974).
- ²⁵W. Zawadzki, and J. Wlasak, *J. Phys. C* **9**, L663 (1976).
- ²⁶L. J. Neuringer, *Proceedings of the Ninth International Conference on the Physics of Semiconductors, Moscow, 1968* edited by S. M. Ryvkin (Nauka, Lenin-
grad, 1968), p. 715.
- ²⁷M. von Ortenberg, *J. Phys. Chem. Solids* **34**, 397 (1973); For the influence of B on screening see P. R. Wallace, *J. Phys. C* **7**, 1136 (1974).
- ²⁸H. Miyazawa, *J. Phys. Soc. Jpn.* **26**, 700 (1969).
- ²⁹M. H. Weiler, R. W. Bierig, and B. Lax, *Phys. Rev.* **184**, 709 (1969).
- ³⁰S. K. Manlief and E. D. Palik, *Solid State Commun.* **12**, 1071 (1973).
- ³¹P. E. Simmonds, J. M. Chamberlain, R. A. Hault, R. A. Stradling, and C. C. Bradley, *J. Phys. C* **7**, 4164 (1974).
- ³²C. P. Pidgeon, S. H. Groves, and J. Feinlieb, *Solid State Commun.* **5**, 677 (1961).
- ³³R. L. Aggarwal, in *Semiconductors and Semimetals*, edited by R. K. Willardson and A. C. Beer (Academic, New York, 1972), Vol. 9, p. 151.
- ³⁴V. Roberts and J. E. Quarrington, *J. Electron.* **1**, 152 (1955).
- ³⁵E. J. Johnson, *Phys. Rev. Lett.* **19**, 352 (1967).
- ³⁶S. Zwerdling, W. H. Kleiner, and J. P. Theriault, *J. Appl. Phys. Suppl.* **32**, 2118 (1961).
- ³⁷C. R. Pidgeon and S. H. Groves, *Phys. Rev.* **186**, 824 (1969).
- ³⁸G. Dresselhaus, A. F. Kip, C. Kittel, and C. Wagoner, *Phys. Rev.* **98**, 556 (1955).
- ³⁹B. Lax, J. G. Mavroides, H. J. Zeiger, and R. J. Keyes, *Phys. Rev.* **122**, 31 (1961).
- ⁴⁰E. D. Palik, G. S. Picus, S. Teitler, and R. F. Wallis, *Phys. Rev.* **122**, 475 (1961).
- ⁴¹R. B. Dennis, Ph.D. thesis (Reading, 1969) (unpublished).
- ⁴²C. R. Pidgeon, D. L. Mitchell, and R. N. Brown, *Phys. Rev.* **154**, 737 (1967).
- ⁴³R. L. Bell, *Phys. Rev. Lett.* **9**, 52 (1962).
- ⁴⁴R. A. Isaacson, *Phys. Rev.* **169**, 312 (1968).
- ⁴⁵J. Konopka, *Phys. Rev. Lett.* **24**, 666 (1970).
- ⁴⁶C. Herman, G. Lampel, and C. Weisbuch, *Proceedings of the Thirteenth International Conference on the Physics of Semiconductors, Rome, 1976*, edited by F. G. Fumi (Tipografia Marves, Rome, 1976), p. 130; C. Herman and C. Weisbuch, *Phys. Rev. B* **15**, 823 (1977).
- ⁴⁷R. Grisar and H. Wachernig, *Appl. Phys.* **12**, 1 (1977).
- ⁴⁸B. D. McCombe and R. J. Wagner, in *Adv. Electron. Electron Phys.* **37**, 1 (1975); **38**, 1 (1975), and references cited therein.
- ⁴⁹R. C. Enck, A. L. Saleh, and H. Y. Fan, *Phys. Rev.* **182**, 790 (1969).
- ⁵⁰B. D. McCombe, R. J. Wagner, S. Teitler, and J. J. Quinn, *Phys. Rev. Lett.* **28**, 37 (1972).
- ⁵¹K. L. Ngai and J. J. Quinn, *Proceedings of the Eleventh International Conference on the Physics of Semiconductors, Warszawa, 1972*, edited by M. Miasek (PWN, Warszawa, 1972), p. 335.
- ⁵²J. Mycielski, G. Bastard, and C. Rigaux, *Phys. Rev. B* **16**, 1675 (1977).
- ⁵³S. J. Miyake, *J. Phys. Soc. Jpn.* **35**, 551 (1973).
- ⁵⁴B. D. McCombe (private communication).
- ⁵⁵S. Morita, S. Takano, and H. Kawamura, *J. Phys. Soc. Jpn.* **39**, 1040 (1975).
- ⁵⁶S. Morita, Ph.D. thesis (Osaka, 1975) (unpublished).
- ⁵⁷F. G. Bass and J. B. Levinson, *Sov. Phys.-JETP* **22**, 635 (1966).
- ⁵⁸E. J. Johnson, J. de Sitter, J. T. Devreese, and K. L. Ngai, *Proceedings of the Thirteenth International Conference on the Physics of Semiconductors, Rome, 1976*, edited by F. G. Fumi (Tipografia Marves, Rome, 1976), p. 1027.
- ⁵⁹W. Zawadzki, R. Grisar, H. Wachernig, and G. Bauer, *Solid State Commun.* **25**, 775 (1978).
- ⁶⁰J. Wlasak and W. Zawadzki in *Proceedings of the Fourteenth International Conference on the Physics of Semiconductors, Edinburgh, 1978* (unpublished).